Journal of Catalysis **203,** 122–132 (2001)
doi:10.1006/jcat.2001.3321, available online at http://www.idealibrary.com on IDEAL®

Hydrogenation and Ring-Opening of Tetralin on Ni and NiMo Supported on Alumina-Pillared α-Zirconium Phosphate Catalysts. A Thiotolerance Study

R. Hernández-Huesca, J. Mérida-Robles, P. Maireles-Torres, E. Rodríguez-Castellón, and A. Jiménez-López[1]

Departamento de Química Inorgánica, Cristalografía y Mineralogía, Facultad de Ciencias, Universidad de Málaga, 29071 Málaga, Spain

Received February 21, 2001; revised June 18, 2001; accepted June 27, 2001

Two different nickel supported on alumina-pillared α-zirconium phosphate materials with metal loading of 20 and 30 wt% have been prepared. In both cases, before reduction, the typical lines of NiO are observed in the XRD patterns. The reduced catalysts exhibit similar metallic area and dispersion values. On the other hand, the catalyst with 20 wt% Ni has the highest surface acidity. Two other NiMo catalysts with 20 wt% Ni and 5 or 10 wt% Mo have been also synthesized. Their XRD patterns show the presence of the $NiMoO_4$ spinel together with an excess of the NiO phase. XPS analysis reveals the existence, in both samples, of 51 and 76% Ni as spinel. After reduction, all these catalysts were tested in the hydrogenation and ring-opening of tetralin at 6.0 MPa. The catalyst with the lowest Ni content (20 wt%) is very active at 623 K, with a conversion of 85% and a high yield of decalins (40%) and cracking compounds (CC) (close to 45%). However, these catalysts strongly deactivate in the presence of 1000 ppm of dibenzotiophene (DBT) in the feed. The incorporation of molybdenum to these catalysts (Ni : Mo weight ratios of 20 : 5 and 20 : 10) favours the ring-opening to the detriment of the hydrogenation process, attributable to new acid sites associated with the molybdenum species. In addition, the NiMo-20 : 10 catalyst exhibits a high thiotolerance in the presence of 1000 ppm of DBT, maintaining its activity after 7 h of time on stream, with a conversion higher than 65% and with good yield of decalins (45%), and maintaining an interesting yield of cracking compounds (18%). © 2001 Academic Press

Key Words: **hydrogenation of tetralin; ring-opening; nickel; molybdenum; pillared phosphates; sulfur tolerance.**

INTRODUCTION

The current high demand for middle distillates for diesel applications and the stringent environmental legislation directed at a reduction in aromatics and sulfur contents of diesel are the reasons for the many studies aimed at the preparation of new catalyst systems. Among these, the most commonly used are monometallic and bimetallic systems (1–5), and mixed sulfides (CoMo, NiW, NiMo) (6–17) supported on alumina and zeolites. On the other hand, studies of nickel on very different supports in hydrogenation reactions (18–23) have shown the importance of these in determining the essential characteristics of the active metal phase. Ni loaded on dealuminated Y-zeolites exhibit excellent catalytic activities in the hydrocracking, hydrodenitrogenation (HDN), and hydrodesulfurization (HDS) reactions of vacuum gasoil at 573–653 K, under pressure (21). Moreover, Chaudhuri *et al.* (22) studied the catalytic hydrogenation of benzene as a model reaction using supported nickel catalysts and they found the best activity for Ni when supported on α-Al_2O_3 with a concentration of 40% Ni (as oxide), with a particle size of 19.6 nm and a metal area of 10.8 $m^2\,g^{-1}$. However, these systems sometimes showed low hydrogenation activities due to strong nickel–support interactions, especially with alumina supports.

In order to reduce these strong interactions, we recently reported the use of fluorinated alumina-pillared α-zirconium phosphate as support for Ni and NiMo, which showed an excellent activity in the benzene hydrogenation reaction (100% conversion to cyclohexane at 773 K) (24) and a high stability for thiophene HDS in the case of NiMo catalysts (25). NiMo-impregnated pillared bentonite has been used for hydrogenation–hydrocracking of vacuum gasoil feedstocks (26). Nickel supported on fluorinated alumina-pillared α-metal(IV) phosphate materials also exhibits good catalytic activity in other reactions such as hydrogenation of nitriles (27).

However, nickel catalysts showed a strong deactivation in the thiophene HDS reaction (21, 28). For this reason, Poels *et al.* (28) studied the deactivation of nickel hydrogenation catalysts by aromatic sulfur compounds, and they concluded that the deactivation results from formation of a surface sulfide which blocks the active sites, and that the thioresistance of nickel catalysts was determined by the nickel surface area per unit weight of catalyst. But after the addition of molybdenum, the catalysts exhibited thioresistance due to the promotion of Ni. Many extensive studies have been carried out to develop thiotolerance in NiW (15) and NiMo (29) catalysts using dibenzothiophene (DBT) or benzothiophene for sulfur poisoning.

[1] To whom correspondence should be addressed. Fax: (+34) 952 132000. E-mail: ajimenezl@uma.es.

0021-9517/01 $35.00

Finally, to study the hydrogenation activity, a model compound is necessary which resembles the structure of aromatic compounds present in the diesel fraction such as light cyclic oil (LCO), where monoaromatics are predominant. Hence, several authors have studied the hydrogenation of tetralin for such model reaction (2, 4, 8, 15, 30, 31). DBT was selected as a sulfur-poisoning agent because it is one of the main sulfur-containing compounds in diesel and its desulfurization chemistry is known (32). The aim of the present work is to evaluate the catalytic behaviour of Ni and NiMo supported on alumina-pillared α-zirconium phosphate in the hydrogenation and ring-opening of tetralin. The thiotolerance of these catalysts was also studied. The catalysts were characterised by XRD, XPS, temperature-programmed reduction with H_2 (H_2-TPR), temperature-programmed desorption of ammonia (NH_3-DTP), H_2 and O_2 chemisorption, and TEM. The catalytic hydrogenation was performed in a continuous fixed-bed reaction system at 523–673 K and 6.0 MPa of H_2 pressure.

EXPERIMENTAL

A porous fluorinated alumina-pillared α-zirconium phosphate, prepared as described elsewhere (33), was chosen as the support. This support has an empirical formula $Zr[Al_{3.39}O_{1.12}(OH)_{1.60}F_{4.90}]H_{0.57}(PO_4)_2$ and is hereafter called AlZrP. Different nickel loadings (20 and 30 wt%) were incorporated on the support by the incipient wetness impregnation method, using ethyl alcohol solutions of $Ni(NO_3)_2$. These catalysts were labelled Ni-20 and Ni-30, respectively. Two additional Ni–Mo catalysts were prepared using ethyl alcohol solutions of $Ni(NO_3)_2$ and $(NH_4)_6Mo_7O_{24}\cdot 4H_2O$, with a nickel loading of 20 wt% and molybdenum loadings of 5 and 10 wt% (NiMo-20 : 5 and NiMo-20 : 10, respectively). All samples were calcined in air at 723 K for 5 h and, prior to any measurement, reduced *in situ* with H_2 (flow rate 60 cm^3 min^{-1}) at 723 K for 1 h, with a heating rate of 15 K min^{-1}.

Powder diffraction patterns (XRD) were obtained with a Siemens D5000 diffractometer, equipped with a graphite monochromator and using Cu $K\alpha$ radiation. X-ray photoelectron spectra were collected using a Physical Electronics PHI 5700 spectrometer with nonmonochromatic Mg $K\alpha$ radiation (300 W, 15 kV, 1253.6 eV). High-resolution spectra were recorded at a 45° take-off angle by a concentric hemispherical analyser operating in the constant pass energy mode at 29.35 eV, using a 720-μm-diameter analysis area. Under these conditions the Au 4$f_{7/2}$ line was recorded with 1.16 eV FWHM at a binding energy of 84.0 eV. The spectrometer energy scale was calibrated using Cu 2$p_{3/2}$, Ag 3$d_{5/2}$, and Au 4$f_{7/2}$ photoelectron lines at 932.7, 368.3, and 84.0 eV, respectively. Charge referencing was measured against adventitious hydrocarbon (C 1*s* 284.8 eV) (34). Samples were mounted on a sample holder without adhesive tape and kept overnight under high vacuum in the preparation chamber before they were transferred to the analysis chamber of the spectrometer. Each region was scanned using several sweeps until a good signal-to-noise ratio was observed. Survey spectra in the range 0–1200 eV were recorded at a 187.85 eV pass energy. The pressure in the analysis chamber was maintained below 5×10^{-6} Pa. A PHI ACCESS ESCA-V6.0 F software package was used for acquisition and data analysis. A Shirley-type background was subtracted from the signals. Recorded spectra were always fitted using Gauss–Lorentz curves in order to determine the binding energy of the different element core levels more accurately. The atomic concentration percentages of the different elements present on the catalysts, before and after the catalytic reaction, were determined by considering the corresponding area sensitivity factor for the different spectral regions measured (34).

The hydrogen temperature-programmed reduction study (H_2-TPR) of supported catalysts was performed between 313 and 973 K, using a flow of Ar/H_2 (40 cm^3 min^{-1}, 10 vol% of H_2) and a heating rate of 10 K min^{-1}. The water produced in the reduction reaction was eliminated by passing the gas flow through a cold finger (193 K). The consumption of H_2 was controlled by an on-line chromatograph provided with a TC detector. NH_3-TPD was used to determine the total acidity of the samples. Before the adsorption of ammonia at 373 K, the samples were heated at 673 K in a He flow. The ammonia desorbed between 373 and 673 K (heating rate of 10 K min^{-1}) was analysed by an on-line gas chromatograph (Shimadzu GC-14A) provided with a TC detector. The surface areas of the catalysts were evaluated from the nitrogen adsorption–desorption isotherms at 77 K in a conventional volumetric apparatus (after degassing at 473 K and 1.33×10^{-2} Pa, overnight).

Hydrogen chemisorption was performed in a conventional volumetric apparatus, after reduction *in situ* of catalysts at 723 K (10 K min^{-1}) for 3 h, under a flow of 40 cm^3 min^{-1} H_2/He (10 vol% H_2). After reduction, catalysts were degassed at 10^{-4} Pa for 16 h at the same temperature and cooled at 298 K, to carry out chemisorption of H_2. The range of pressure studied in the chemisorption was 0.05–1.00 Pa and the amounts of hydrogen chemisorbed were calculated by extrapolation of the isotherms to zero pressure (35). Under the same experimental conditions, consumption of H_2 was nil on the support. Oxygen chemisorption was carried out after hydrogen chemisorption. The sample was again degassed at 10^{-4} Pa for 16 h at 723 K. After cooling, the oxygen chemisorption was carried out at 673 K up to an equilibrium pressure of 5.00–6.00 Pa. The uptake due to oxygen chemisorbed was determined by extrapolation of the isotherm at zero pessure and considering that all the metallic nickel of the catalyst reacts with oxygen to form NiO at 673 K (36). TEM micrographs were obtained with

a Phillips CM-20 high-resolution transmission electron microscope equipped with an EDAX microanalysis system. Previously reduced samples were dispersed in *n*-heptane and suspended on a Cu grid of 3.5 mm diameter.

Activity Measurements

The hydrogenation of tetralin was performed in a high-pressure fixed-bed continuous-flow stainless steel catalytic reactor (9.1 mm i.d. and 230 mm length) operated in the down-flow mode. The reaction temperature was measured with an interior placed thermocouple in direct contact with the top part of the catalyst bed. The organic feed consisted of a solution of tetralin in *n*-heptane (10 vol%) and was supplied by means of a Gilson 307SC piston pump (model 10SC). The thiotolerance of the catalysts was evaluated by adding two different amounts of DBT (300 and 1000 ppm for normal and severe sulfur poisoning tests, respectively) to the organic feed. A fixed volume of catalyst (3 cm^3 with particle size of 0.85–1.00 mm) without dilution was used in all the studies. Prior to the activity test, the catalysts were reduced *in situ* at atmospheric pressure with H_2 (flow rate 60 cm^3 min^{-1}) at 723 K for 1 h, with a heating rate of 15 K min^{-1}. Catalytic activities were measured at different temperatures, under 6.0 MPa hydrogen pressure, and a liquid hourly space velocity (LHSV) of 6.0, 9.0, and 11.4 h^{-1}. The H_2/tetralin molar ratio was 10.1, 14.4, and 19.2. The reaction was kept at steady state for 3 h, and liquid samples were collected and kept in sealed vials for posterior analysis by both mass spectrometry (Hewlett-Packard 5988A) and gas chromatography (Shimadzu GC-14B, equipped with a flame ionisation detector and a capillary column (TBR-1)). First, the influence on the conversion and selectivity of reaction parameters such as reaction temperature, contact time, and H_2/tetralin molar ratio was studied to optimise the reaction conditions. The performance of the microreactor and the accuracy of the analytical method were studied by feeding a solution of tetralin in *n*-heptane (10 vol%) to the reactor filled with 3 cm^3 of SiC, operating at 573 K and 6.0 MPa. No formation of foreign products was detected with a recovery percentage of the tetralin feed of 95%. In previous experiments, the variation of the amount of catalysts and the total flow rate maintaining constant the space velocity led to no modification of conversion values. No influence with the particle diameter was found either.

RESULTS AND DISCUSSION

Characteristics of Catalysts

The powder XRD patterns of the unreduced supported nickel catalysts show the characteristic diffraction signals of NiO (2.41, 2.09, and 1.48 Å), whose intensity increases with nickel loading. Upon reduction, the reflections at 2.03 and 1.74 Å, typical of metallic nickel, appear. However, the addition of molybdenum gives rise to the formation

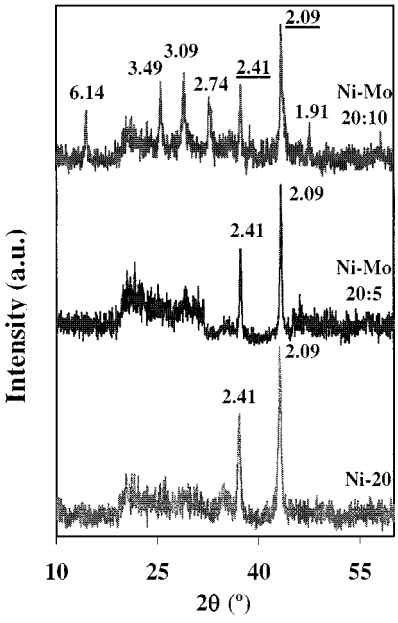

FIG. 1. XRD patterns of Ni and NiMo supported samples before reduction.

of the $NiMoO_4$ spinel, which is clearly observed in NiMo-20 : 10 with diffraction lines at 6.14, 3.49, 3.09, 2.74, 2.06, and 1.91 Å (37), but the presence of NiO is still observed (Fig. 1). The incorporation of these oxides onto the AlZrP support ($S_{BET} = 135$ m^2 g^{-1}) provokes a severe decrease in the specific surface area (Table 1), up to 60% in the case of the sample with the highest nickel content, Ni-30. However, no significant changes in the surface area were observed after reduction, except in the case of the NiMo-20 : 10 catalyst, where the S_{BET} increased from 56 to 84 m^2 g^{-1}.

Concerning the acid properties of this family of catalysts, the presence of nickel and molybdenum oxides provokes a remarkable decrease in the total acidity values (Table 1), as determined by NH_3-DTP, in comparison with that of the support (1115 μmol g^{-1}). These metal oxides probably hinder the access of ammonia to the acid centres located into the micropores and, at the same time, could cover acid sites of the support.

TABLE 1

Textural and Acid Characteristics of Ni and NiMo Catalysts, before and after Reduction

Catalyst	*M* (wt%)	S_{BET} (m^2 g^{-1}) Unreduced	S_{BET} (m^2 g^{-1}) Reduced	Total acidity (μmol NH_3 des. g^{-1})
Ni-20	19.6	74	69	447
Ni-30	29.3	54	45	290
NiMo-20 : 5	19.5 : 4.8	73	75	696
NiMo-20 : 10	19.9 : 9.7	56	84	395

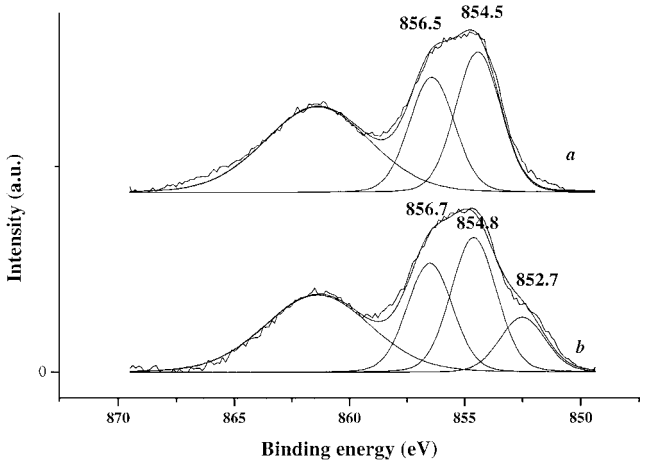

FIG. 2. Ni $2p_{3/2}$ XPS spectra of Ni-30: (a) before and (b) after reduction.

X-ray photoelectron spectroscopy has also been used in order to get valuable information about the electronic nature of the nickel and molybdenum surface species. The Ni $2p_{3/2}$ core level spectra of the Ni-30 catalyst, before and after reduction, are shown, as a representative example, in Fig. 2. The spectrum of the unreduced catalyst exhibits a broad asymmetric band, characteristic of Ni(II) species, which becomes wider as the nickel loading increases, indicating the existence of Ni(II) in distinctive environments. This broad signal can hence be deconvoluted into two peaks with their maxima at binding energies of 854.5 and 856.5 eV, respectively. These values indicate that Ni(II) is located in both the octahedral holes of the supported NiO structure and the tetrahedral positions of a $NiAl_2O_4$ spinel structure formed by diffusion of Ni(II) ions into the alumina pillars (38). The binding energy at 862 eV corresponds to the shake-up satellite structure of Ni(II). The percentage areas of each contribution in the unreduced catalysts are listed in Table 2. As expected, by increasing the nickel loading, the NiO percentage is increased with respect to that of nickel in a spinel structure (25, 26).

After reduction, the Ni $2p_{3/2}$ XPS spectrum shows a shoulder at a lower binding energy (852.7 eV) that corresponds to the presence of Ni^0 (Fig. 2). As a consequence of the strong interaction of the active phase with the support, only a portion of supported nickel oxide is reduced to a metallic state and most of the nickel remains as Ni(II). The Mo 3*d* core-level XPS spectra of the unreduced supported NiMo catalysts show the Mo $3d_{5/2}$ and Mo $3d_{3/2}$ doublet at 232.1 and 235.2 eV, respectively. The Mo $3d_{5/2}$ value is very close to those observed for MoO_3 (232.6 eV) and $NiMoO_4$ spinel (232.5 eV). The symmetry of the Mo $3d_{5/2}$ peak indicates the existence of only one type of molybdenum ($NiMoO_4$), as observed by XRD. For NiMo-containing samples, the surface Ni/Al atomic ratios (Table 2) are higher than that corresponding to Ni-20, indicating a preferential location of nickel ions on the surface, forming such $NiMoO_4$ spinel. This is in agreement with the existence of two values for Ni $2p_{3/2}$ at 854.5 and 856.2 eV, assigned to NiO and $NiMoO_4$, respectively, increasing the proportion of the latter with molybdenum loading. However, the formation of $NiAl_2O_4$ spinel cannot be ruled out.

TABLE 2

Binding Energies (eV) and Surface Atomic Ratios of Unreduced Ni and NiMo Catalysts

	NiO		Spinel				
	Ni $2p_{3/2}$		Ni $2p_{3/2}$			Mo $3d_{5/2}$	
Catalyst	B.E. (eV)	%	B.E. (eV)	%	Ni/Al	B.E. (eV)	Ni/Mo
Ni-20	854.5	47	856.5	53	0.17	—	—
Ni-30	854.5	53	856.6	47	—	—	—
NiMo-20 : 5	854.5	49	856.6	51	0.34	232.2	2.20
NiMo-20 : 10	854.5	24	856.2	76	0.32	232.1	0.90

The XPS spectra of NiMo catalysts, after reduction, corresponding to the Mo 3*d* core level are shown in Fig. 3. From the appearance of the doublets at 229.4–232.6 and 231.9–234.8 eV in these spectra, the coexistence of Mo^{IV} and Mo^{VI} is deduced, respectively, in agreement with the results found from TPR analysis (*vide infra*). In the Ni 2*p* core level (Fig. 3) Ni^{2+} at 855.7 eV, forming a $NiMoO_4$ spinel, and Ni^0 at 852.1 eV, are detected.

The H_2-TPR profiles of the supported Ni and NiMo catalysts are shown in Fig. 4. For comparison, the H_2-TPR profile of MoO_3 is also included. It can be observed that the range of hydrogen consumption depends on the nickel loading, in such a way that the sample with the lowest nickel content presents an intense broad peak with a maximum at 688 K. At a higher nickel content, this maximum shifts to lower reduction temperatures. In all cases, reduction temperatures higher than those observed for bulk NiO (613 K) imply the existence of an interaction between the Ni(II) species and the support, as revealed by XPS studies. The percentage of Ni interacting with the support is low for higher nickel loading, thus favouring the reducibility of Ni(II). An additional reduction peak is also observed at higher temperatures (773–823 K), which can be assigned to the reduction of the Ni(II) forming part of the $NiAl_2O_4$ spinel (39–42).

In the H_2-TPR profiles of the supported NiMo catalysts, a shift to higher temperatures for the Ni(II) reduction peaks was observed, due to nickel being present mainly as a $NiMoO_4$ spinel. Thus, the H_2-TPR profile of the NiMo-20 : 5 sample shows a broad peak which could include the reduction of both types of nickel, NiO and $NiMoO_4$. This effect is more clearly seen in the H_2-TPR profile of the NiMo-20 : 10 sample, where two peaks of hydrogen consumption at 653 and 778 K were observed. On the other hand, in the temperature range studied, only the reduction of Mo(VI) to

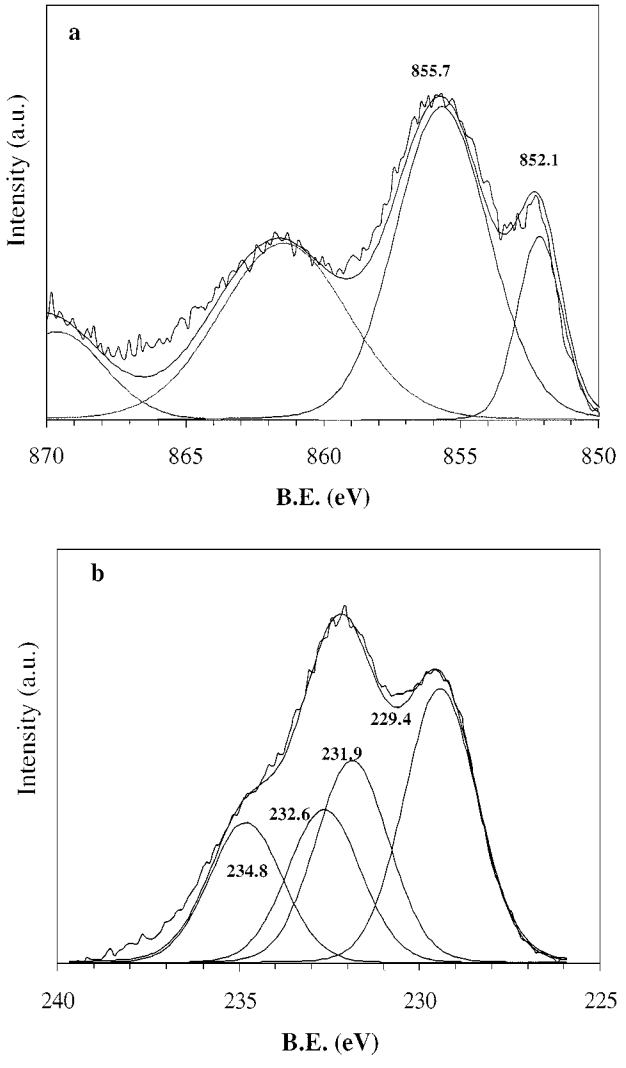

FIG. 3. Ni $2p_{3/2}$ (a) and Mo 3*d* (b) XPS spectra of reduced NiMo-20 : 10 catalyst.

Mo(IV) takes place (953 K) in the case of bulk MoO_3 (43). However, the H_2-TPR profiles of the studied NiMo catalysts do not clearly show any peak corresponding to the reduction of molybdenum, although a shoulder at 883 K could be assigned to the partial reduction of Mo(VI) to Mo(IV) in both catalysts, as has been detected by XPS analysis.

The reduction degree of catalysts, α, as determined by oxygen chemisorption at 673 K, increases with nickel content (Table 3). This is due to the presence of greater amounts of exposed NiO which does not interact with the support. Nevertheless, complete reduction was not achieved for any sample. Moreover, α is higher for NiMo catalysts; therefore, nickel in a $NiMoO_4$ spinel is more reducible.

On the other hand, the dispersion degree (D), the metallic surface, and the particle size of the different catalysts were determined using the hydrogen chemisorption data (Table 3). The metallic dispersion is, in general, low, because the high nickel loadings used in the present work favour particle agglomeration. Thus, the dispersion values are similar to those found for nickel supported on alumina catalysts (44), but slightly lower than those obtained on other supports (45–47). However, the incorporation of molybdenum into these catalysts slightly ameliorates the dispersion, probably due to the interaction between Mo ions and Ni^0 particles which reduces the sintering. The particle sizes increase with the nickel content, but the incorporation of molybdenum produces a reduction in the particle size as a result of the above-mentioned interaction.

Further, the Ni and NiMo catalysts were also studied by TEM in order to estimate the metallic particle size. It can be seen that the micrographs of the reduced Ni-20 and NiMo-20 : 10 catalysts (Fig. 5) show metallic particles with a broad range of sizes, which is to be expected given the heterogeneous nature of the support used in the present study. Nevertheless, the average particle sizes, according to H_2 chemisorption, match very well with the sizes observed in the micrographs (Table 3).

Catalytic Results

A preliminary analysis of the liquid products, obtained in the catalytic hydrogenation of tetralin on the reduced

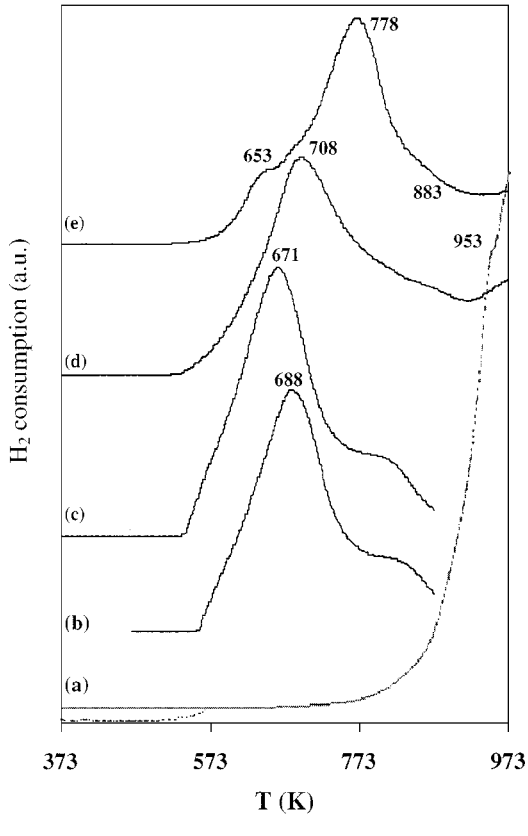

FIG. 4. H_2-TPR profiles of (a) bulk MoO_3 and of oxide supported (b) Ni-20, (c) Ni-30, (d) NiMo-20 : 5, and (e) NiMo-20 : 10.

TABLE 3

Surface Characteristics of the Ni and NiMo Catalysts

Catalyst	O_2 chemisorbed (μmol/g)	α reduction degree	H_2 chemisorbed (μmol/g)	D (%), metallic dispersion	S_{met}, metallic, surface (m^2/g)	d (nm), average particle diameter	
						H_2	TEM
Ni-20	1126	0.66	5.32	1.05	7	40	35
Ni-30	1814	0.71	8.17	1.0	6.7	46	40
NiMo-20 : 5	1346	0.79	10.2	1.7	11	30	25
NiMo-20 : 10	1405	0.83	8.5	1.35	9	39	30

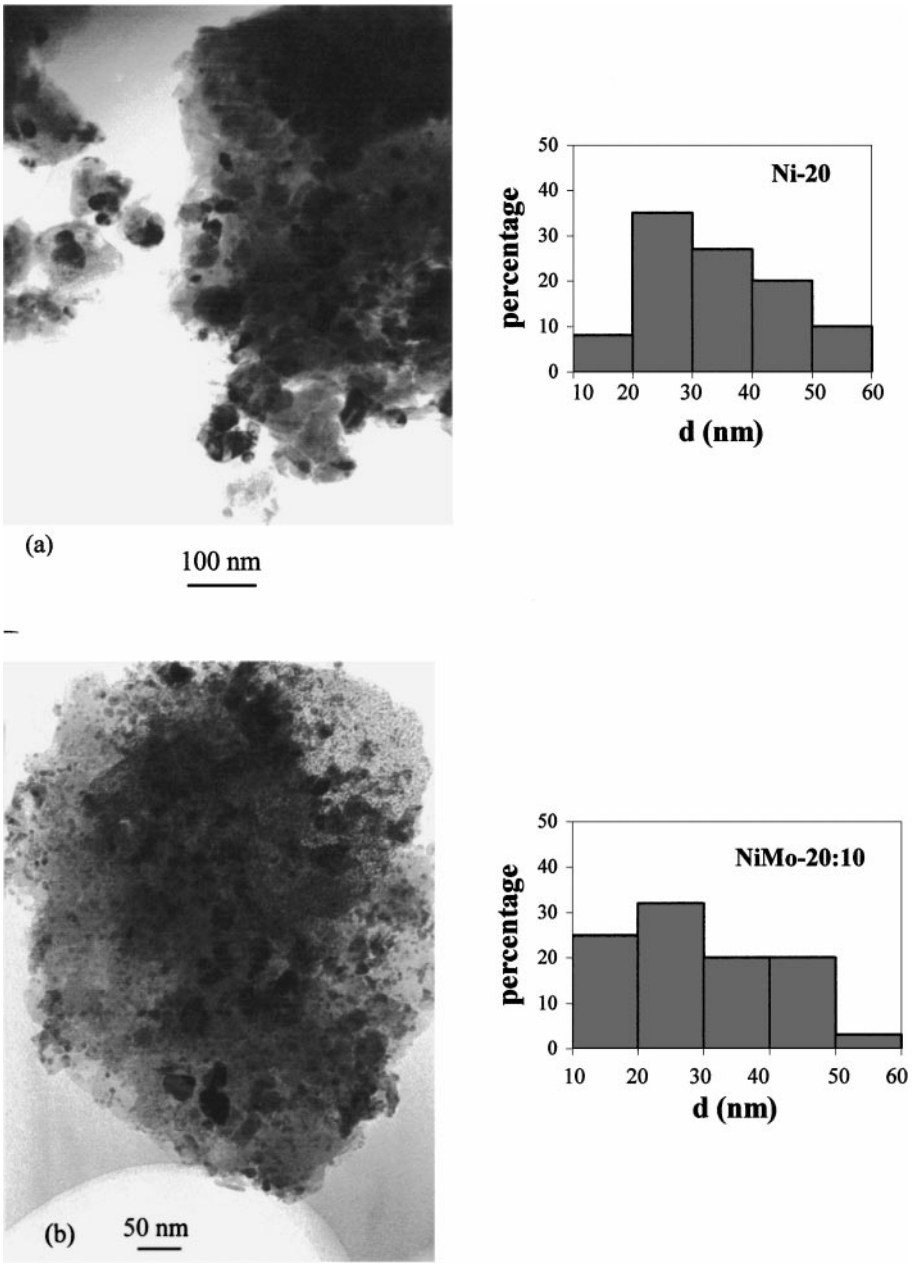

FIG. 5. Transmission electron micrographs and histograms of particle size of (a) Ni-20 and (b) NiMo-20 : 10 catalysts.

Ni and NiMo catalysts by GC/MS, identified the presence of more than 70 compounds. The study of the product distribution required the following classification: *cis*-decalin, *trans*-decalin, naphthalene, volatile compounds (VC), and cracking compounds (CC). The CC group includes many different compounds, most of which find their origin in the ring-opening of tetralin such as benzene, alkylbenzenes (toluene, ethylbenzene, xylene, *n*-propylbenzene, *n*-butylbenzene, isopropylbenzene), polyalkylolefins, and others such as indan. The noncondensable products, C_1–C_4, were included in the VC group, and were calculated from the carbon balance of the reaction. Products heavier than decalins were not found.

Concerning the evolution of the conversion (calculated as the percentage of tetralin converted) as a function of the reaction temperature (Fig. 6), until 623 K, the supported nickel catalysts exhibit a similar catalytic behaviour, with conversion values higher than 85%, but falling at higher temperatures. These similar conversions were expected owing to the analogous metallic areas and dispersions of these catalysts. With regard to the yields of the different compounds, it is observed that the formation of *trans*-decalin is favoured at low temperatures. By increasing the reaction temperature, an increase in the yield of CC was found, but to the detriment of *trans*-decalin. This behaviour was expected taking into account the exothermic character of the hydrogenation of tetralin, which is favoured at low temperatures (2, 3, 48, 49). In contrast, the cracking reactions will be favoured at high temperatures due to their endothermic character (8). By comparing the two supported nickel catalysts, up to 623 K the CC production is seen to be higher for the lowest nickel content, which agrees well with its higher acidity (Table 1). The yield of volatile compounds (VC) is close to 20% at 673 K for the Ni-30 catalyst, giving rise to a decrease in the yield of hydrogenation products. In both cases, naphthalene was also detected at high temperatures. On the basis of these results, a temperature of 623 K was selected for further experiments. At this temperature, the conversion of tetralin is still high, together with a good yield of CC and a very low yield of VC.

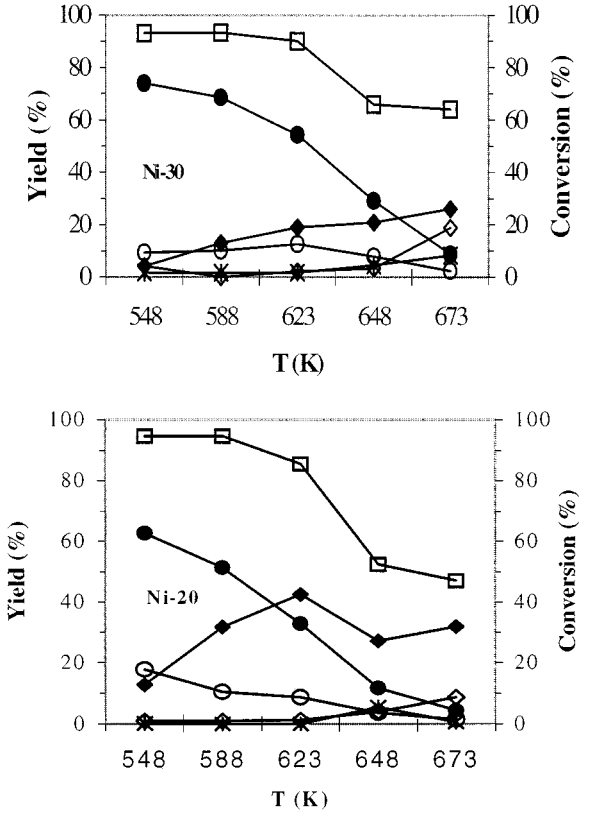

FIG. 6. Variation of the conversion (□) and yield for tetralin hydrogenation reaction as a function of the reaction temperature for the supported nickel catalysts. Yield: (●) *t*-decalin, (○) *c*-decalin, (*) naphthalene, (◆) CC, and (◇) VC. Experimental conditions: 6.0 MPa, LHSV = 6 h^{-1}, GHSV = 1500 h^{-1}, H_2/THN molar ratio = 14.4.

On the other hand, reaction temperatures higher than 623 K are usual in hydrotreating processes; consequently, high concentrations of H_2 are necessary to overcome the thermodynamic limitations (2). This implies elevated costs to recycle the excess of H_2; so, an optimisation study was carried out to find the adequate H_2/tetralin molar ratio. The tetralin conversion on the Ni-30 catalyst at 623 K rises by increasing the H_2/tetralin molar ratio from 10.1 to 19.2, together with a slight increment in the *trans*-decalin production. However, in both catalysts, the tetralin conversions are close to 90% with a H_2/tetralin molar ratio of 14.4 (data at 623 K in Fig. 6). But, under these conditions, the Ni-20 catalyst is more selective for cracking compounds with a yield of 45%. This catalyst exhibits a high conversion with an adequate balance between hydrogenation and cracking compounds.

Although the Ni-30 catalyst has a high hydrogenation activity, the Ni-20 catalyst exhibits not only this behaviour but also a higher selectivity toward CC. This performance could be due to the higher acidity of the Ni-20 catalyst (Table 1), which favours the ring-opening of decalins and tetralin. These results agree well with those reported for Pd/Pt catalysts supported on zeolites with different acidities (8). Other authors have also found that the acidity of the catalyst is a key factor in the hydrocracking process (5, 50–53). Li *et al.* (50, 51) studied Ni and NiMo catalysts supported on a physical mixture of alumina and zeolite USY in the hydrocracking reaction of diphenylmethane, and they found that the hydrocracking activity increased with acidity.

The effect of the addition of Mo (5 and 10 wt%) to the Ni-20 catalyst on its performance in the catalytic hydrogenation of tetralin (conversion, selectivity and thiotolerance) was also evaluated. The reaction was carried out using the conditions employed for the Ni-20 catalyst (H_2 flow = 75 mL min^{-1}, H_2/THN molar ratio = 14.4, H_2 pressure = 6 MPa, LHSV = 6 h^{-1}, GHSV = 1500 h^{-1}, contact time = 2.4 s and 623 K). The conversion of tetralin was slightly higher than those observed for the nickel

TABLE 4

Conversions, Selectivities, and Yields of the Catalytic Reaction of Tetralin on the Ni-20 and the NiMo Catalysts in the Presence of DBT

	DBT (ppm)			
	0	300	1000	Regeneration
NiMo-20 : 5				
Conversion (%)	94.8	81.2	42.4	20.6
Selectivity (%)				
t-Decalin	31.9	53.0	41.6	31.5
c-Decalin	4.1	17.4	19.2	18.0
CC	47.5	25.4	23.2	26.9
VC	11.3	4.0	13.6	15.5
Yield (%)				
t-Decalin	30.2	43.0	17.6	6.5
c-Decalin	3.9	14.1	8.1	3.7
CC	45.0	20.6	9.8	5.5
VC	10.7	3.2	5.8	3.2
NiMo-20 : 10				
Conversion (%)	96.4	94.6	65.4	69.0
Selectivity (%)				
t-Decalin	30.4	54.3	51.2	54.6
c-Decalin	4.7	13.3	17.6	17.0
CC	61.1	31.5	27.2	26.1
VC	0.2	0.9	3.2	1.4
Yield (%)				
t-Decalin	29.3	51.4	33.5	37.7
c-Decalin	4.5	12.6	11.5	11.7
CC	58.9	29.8	17.8	18.0
VC	0.2	0.8	2.1	1.0
Ni-20				
Conversion (%)	86.0	27.7	13.9	21.1
Selectivity (%)				
t-Decalin	40.0	27.1	4.7	3.4
c-Decalin	8.0	21.0	3.3	2.7
CC	51.0	32.0	22.6	19.3
VC	0	14.7	46.7	59.0
Yield (%)				
t-Decalin	34.4	7.5	0.6	0.7
c-Decalin	6.9	5.8	0.4	0.6
CC	43.9	8.9	3.1	4.1
VC	0	4.1	6.5	12.4

catalysts (Table 4). However, the yield of decalins decreases with the incorporation of Mo, although, interestingly, the yield of cracking compounds is enhanced with the amount of Mo added. Thus, for NiMo-20 : 5 and NiMo-20 : 10 the yields of cracking compounds are 45 and 59%, respectively. This fact can be attributed to the existence of new Lewis acid sites related to the presence of molybdenum species, which are responsible for the ring-opening reactions.

Thiotolerance

The thiotolerance evaluation of the Ni-20, NiMo-20 : 5, and NiMo-20 : 10 catalysts was carried out by adding different amounts of DBT to the feed, and operating under the same experimental conditions used for the study of the NiMo catalysts. Moreover, the catalyst regeneration was checked at the end of the thiotolerance test by treating the spent catalysts at 723 K under a H_2 flow (60 cm^3 min^{-1}) for 1 h. The Ni-20 catalyst in the presence of 300 ppm of DBT showed a clear deactivation as a function of time on stream, which becomes more severe by increasing the amount of DBT up to 1000 ppm (Fig. 7). Under the latter conditions, the conversion is lowered to 15%, and even though the spent catalyst is treated with a flow of H_2, no significant variation of the catalytic activity operating with a feed free of DBT is observed (conversion of 20%), indicating that an irreversible deactivation of the catalyst has occurred. This deactivation process could occur through the formation of nickel sulfide on the catalyst surface (54), as confirmed by the presence of a S 2*p* peak at a binding energy of 162.3 eV in its XPS spectrum. By TEM, the formation of bigger nickel sulfide particles, with average sizes of 60–80 nm, was also detected.

In the case of supported NiMo catalysts, the conversion decreases only slightly with 300 ppm of DBT in the feed (Table 4). The NiMo-20 : 10 catalyst is of special interest because after 7 h of reaction with a feed containing 300 ppm of DBT, the conversion was almost 95%, similar to the conversion value with the poison-free feed. With 1000 ppm of DBT, both catalysts undergo a lower deactivation than that observed with the catalyst without Mo, especially for the NiMo-20 : 10 catalyst that still maintains a very high conversion (65%), after 7 h of reaction. The better thiotolerance of the NiMo catalysts with respect to the Ni-20 catalyst could be explained by taking into account the different species of Ni^{2+} present in both cases. This would suggest that, in supported nickel catalysts, a fraction of nickel migrates

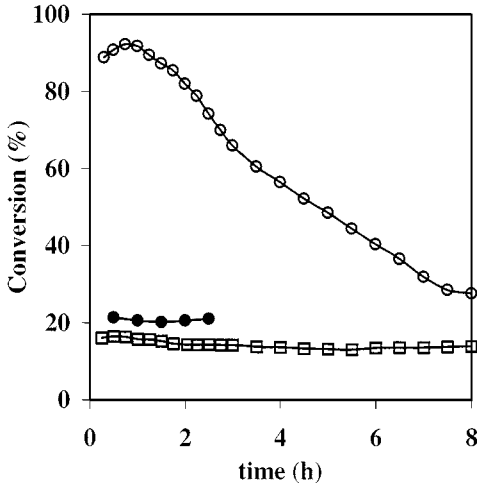

FIG. 7. Plots of tetralin conversion versus time on stream for Ni-20 catalyst in the presence of DBT: (○) 300 ppm, (□) 1000 ppm, and (●) regenerated sample and feed without DBT. Experimental conditions: 6.0 MPa, $T_{reaction}$ = 623 K, LHSV = 6 h^{-1}, GHSV = 1500 h^{-1}, H_2/THN molar ratio = 14.4.

into the tetrahedral holes of the alumina pillars; these ions are neither reducible under the experimental conditions imposed nor located on the external surface, and, in consequence, they do not play any role in the catalytic reactions. In contrast, when Mo is added to the nickel-based catalysts, a NiMoO4 spinel is formed, which favours the formation of the "Ni–Mo–S" structure in the presence of a feed containing DBT (54). This phase is very active in both the HDS of dibenzothiophene and the hydrogenation of aromatic compounds. On the other hand, the excess of nickel used for the preparation of these catalysts justifies the simultaneous presence of Ni^0 and unreduced Ni^{2+} ions on their surface, as observed from XPS studies. The existence of these ions is important because, according to other authors (55, 56), they interact more easily with the sulphur atom of DBT than Ni^0, avoiding, in this way, the poisoning of Ni^0 which remains active for the hydrogenation reaction. Finally, it is noteworthy that the NiMo-20 : 10 catalyst, after regeneration by reduction at 723 K in a H_2 flow for 1 h, still exhibits conversion close 70% after 7 h on stream (Table 4).

Table 4 compiles the selectivities and yields of the different reaction products after 7 h on stream for the NiMo catalysts in the presence of different amounts of DBT in the feed. Both catalysts exhibit an increment in their catalytic activity for the hydrogenation reaction. This fact is concomitant with a decrease in the field of ring-opening products. This variation is less marked for the NiMo-20 : 10 catalyst, in which, after treatment with 1000 ppm of DBT, the yield of CC is 18%, remaining unaffected by time on stream.

In order to obtain more detailed information about the hydrogenation properties of this family of catalysts, the hydrogenation of tetralin was analysed according to the pseudo-first-order kinetic equation (1, 57, 58),

$$k = -\left(\frac{F}{m}\right) \mathrm{Ln}(1 - x),$$

where k is the pseudo-first-order reaction constant (h^{-1}), x is the fraction of hydrogenated tetralin (mol h^{-1}), F is the molar flow of reactant (mol h^{-1}), and m refers to the metal atoms exposed per gram of catalyst (mol g_{cat}^{-1}) determined by hydrogen chemisorption. Figure 8 shows the values of k after 7 h of reaction for the different catalysts studied. From this data, it is possible to conclude that the Ni-20 catalyst exhibits the best activity in the hydrogenation reaction, with a reaction constant of 436 h^{-1}. Both NiMo catalysts exhibit similar hydrogenation activity. When DBT is added to the feed, the hydrogenation constant dramatically decreases for the Ni-20 catalyst, this being lower when the concentration of DBT is increased. In contrast, the opposite is found for NiMo catalysts, since the hydrogenation constant for the NiMo-20 : 10 catalyst rises to 336 h^{-1} with 300 ppm of DBT in the feed. Even with 1000 ppm of DBT, the hydrogenation capacity of this catalyst is very considerable. In the

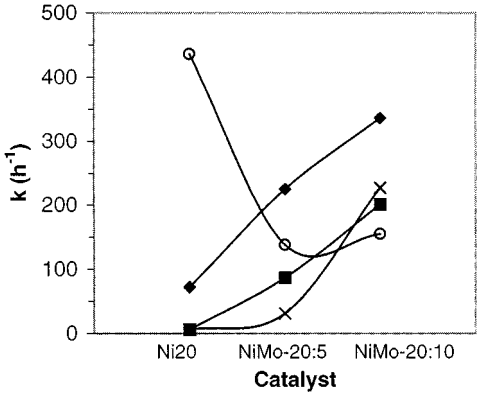

FIG. 8. Evolution of the pseudo-first-order rate constants for tetralin hydrogenation on the Ni20, NiMo-20 : 5, and NiMo-20 : 10 catalysts with the DTB concentration in the feed: (○) 0 ppm, (◆) 300 ppm, (■) 1000 ppm, and (×) regenerated. $P_{reaction} = 6.0$ MPa, $T_{reaction} = 623$ K, LHSV = 6 h^{-1}, GHSV = 1500 h^{-1}, H_2/THN molar ratio = 14.4.

spent catalyst, the formation of sulfide is detected by the appearance of a peak in the core level of S 2p at 162.1 eV, corresponding to either the "Ni–Mo–S" phase or NiS (59). However, in the core level of Mo 3d it is very difficult to detect the formation of the "Ni–Mo–S" structure, because the ranges of binding energies of Mo(IV) oxide and MoS_2 are similar. In any case, from the observed results, the hydrogenation activity of these catalysts could be related to the formation of a "Ni–Mo–S" phase, where Ni adopts a square pyramidal coordination similar to that of the millerite structure (60, 61), which seems to be the active phase in sulfided NiMo catalysts. This assumption is in agreement with the higher conversion of the NiMo-20 : 10 catalyst, where the higher molybdenum loading favours the formation of such structure. The increase in the hydrogenation activity of NiMo catalysts is concomitant with a decrease in the ring-opening reaction leading to cracking compounds. This decreasing could be related to the disappearance of acid sites due to the sulfidation of the Mo(IV) ions, because the formation of cracking compounds, observed in the absence of DBT in the feed, could be associated with the presence of Mo oxide species. After regeneration of spent catalysts by reduction under the same conditions used in the preparation of catalysts, NiMo-20 : 10 exhibits the same hydrogenation constant as the pristine catalyst after treatment with a feed poisoned with 1000 ppm of DBT. The k_s/k ratios corresponding to the hydrogenation constants in the presence of DBT are listed in Table 5. The high values found for the NiMo-20 : 10 catalyst are noticeable, with a k_s/k ratio of 2.17 in the presence of 300 ppm of DBT. Moreover, the regeneration of this catalyst after treatment with a feed containing DBT ameliorates its hydrogenating properties, as revealed by the higher hydrogenation constant ($k_{reg} = 227$).

In conclusion, the NiMo-20 : 10 catalyst exhibits a dual behaviour: a high performance for tetralin hydrogenation in the presence of 1000 ppm of DBT (45% yield) and, at

TABLE 5

Tetralin Hydrogenation Activity of Ni-20 and NiMo Supported on AlZrP Catalysts

Catalyst	ppm DBT	k_s (h^{-1}), 7 h	k_s/k
Ni-20	0	$k = 436$	
	300	72	0.17
	1000	6	0.01
	Reg.	$k_{reg} = 6$	
NiMo-20 : 5	0	$k = 138$	
	300	225	1.63
	1000	87	0.63
	Reg.	$k_{reg} = 31$	
NiMo-20 : 10	0	$k = 155$	
	300	336	2.17
	1000	201	1.30
	Reg.	$k_{reg} = 227$	

the same time, a good activity in the ring-opening reaction leading to cracking compounds (18% yield), thus giving rise to hydrocarbons free of sulfur and compounds such as *cis–trans* decalins, alkyl benzenes, polyalkylolefines, etc. This behaviour could be extrapolated to the use of this catalyst against a light cycle oil (LCO) feedstock where the formation of different compound free of sulfur and corresponding to the diesel fraction with improved cetane number can be expected.

ACKNOWLEDGMENTS

This research was performed under Contract No. BRPR CT97 0560 of the European Union. We also thank the CICYT (Spain) (Project MAT2000-1144) for financial support. R.H.-H. is grateful to the CONACYT (Mexico) for a doctoral fellowship.

REFERENCES

1. Navarro, R. M., Pawelec, B., Trejo, J. M., Mariscal, R., and Fierro, J. L. G., *J. Catal.* **189**, 184 (2000).
2. Fujikawa, T., Idei, K., Ebihara, T., Mizuguchi, H., and Usui, K., *Appl. Catal.* **192**, 253 (2000).
3. Corma, A., Martínez, A., and Martínez-Soria, V., *J. Catal.* **169**, 480 (1997).
4. Kabe, T., Qian, W., Hirai, Y., Li, L., and Ishihara, A., *J. Catal.* **190**, 191 (2000).
5. Chang, J. R., and Chang, S. L., *J. Catal.* **176**, 42 (1998).
6. Sato, K., Iwata, Y., Miki, Y., and Shimada, H., *J. Catal.* **186**, 45 (1999).
7. Sato, K., Iwata, Y., Yoneda, T., Miki, Y., and Shimada, H., *Catal. Today* **45**, 367 (1998).
8. Yasuda, Y., and Yoshimura, Y., *Catal. Lett.* **46**, 43 (1997).
9. Lecrenay, E., Sakanishi, K., Mochida, K., and Suzuka, T., *Appl. Catal. A: General* **175**, 237 (1998).
10. Ozkan, A. R., Yanik, J., Saglam, M., and Yuskel, M., *Energy Fuels* **13**, 433 (1999).
11. Lemberton, J. L., Baudon, A., Guisnet, M., Marchal, N., and Mignard, S., *Stud. Surf. Sci. Catal.* **106**, 129 (1997).
12. Sanford, E. C., Steer, J. G., Muehlenbachs, K., and Gray, M. R., *Energy Fuels* **9**, 928 (1995).
13. Bouchy, M., Peureuxdenys, S., Dyfresnes, P., and Kasztelan, S., *Ind. Eng. Chem. Res.* **32**, 1592 (1993).
14. Lure, M. A., Kurets, I. Z., Kushnarev, D. F., Malyuchenko, A. A., and Schmidt, F. K., *Kinet. Catal.* **41**, 57 (2000).
15. Yasuda, H., Higo, M., Sato, T., Inamura, M., Matsubayashi, H., Shimada, H., Nishijima, A., and Yoshimura, Y., *Catal. Today* **39**, 77 (1997).
16. Chadwick, D., Oen, A., and Siewe, C., *Catal. Today* **29**, 229 (1996).
17. Ho, T. C., *Energy Fuels* **8**, 1149 (1994).
18. Coenen, J. W. E., *Ind. Eng. Chem. Fundam.* **25**, 43 (1986).
19. Ledoux, M. J., "Specialist Periodical Reports, Catalysis," Vol. 7, p. 125. Royal Chem. Soc., London, 1985.
20. Corma, A., Iglesias, M., and Sanchez, F., *Catal. Lett.* **32**, 313 (1995).
21. Isoda, T., Kusakabe, K., Morroka, S., and Mochida, I., *Energy Fuels* **12**, 493 (1998).
22. Chaudhuri, S. N., Nath, S. K., and Majumdar, D. S., *Stud. Surf. Sci. Catal.* **113**, 793 (1998).
23. Zhang, Z. G., Okada, K., Yamamoto, M., and Yoshida, T., *Catal. Today* **45**, 361 (1998).
24. Mérida-Robles, J., Olivera-Pastor, P., Rodríguez-Castellón, E., and Jiménez-López, A., *J. Catal.* **169**, 317 (1997).
25. Mérida-Robles, J., Rodríguez-Castellón, E., and Jiménez-López, A., *J. Mol. Catal. A: Chemical* **145**, 169 (1999).
26. Occelli, L. M., and Rennard, R. J., *Catal. Today* **2**, 309 (1988).
27. Braos-García, P., Maireles-Torres, P., Rodríguez-Castellón, E., and Jiménez-López, A., *J. Mol. Catal. A: Chemical* **168**, 279 (2001).
28. Poels, K., Vanbeek, W. P., Denhoed, W., and Visser, C., *Fuel* **74**, 1800 (1995).
29. Lecrenay, E., Sakanishi, K., and Mocida, I., *Catal. Today* **39**, 13 (1997).
30. Chang, J. R., Chang, S. L., and Lin, T. B., *J. Catal.* **169**, 338 (1997).
31. Yasuda, H., Sato, T., and Yoshimura, Y., *Catal. Today* **50**, 63 (1999).
32. Gates, B. C., Katzer, J. R., and Schuit, G. C. A., "Chemistry of Catalytic Processes," p. 39. McGraw-Hill, New York, 1979.
33. Mérida-Robles, J., Olivera-Pastor, P., Jiménez-López, A., and Rodríguez-Castellón, E., *J. Phys. Chem.* **100**, 14726 (1996).
34. Moulder, J. F., Stickle, W. F., Sobol, P. E., and Bomben, K. D., *in* "Handbook of X-Ray Photoelectron Spectroscopy" (J. Chastain, Ed.). Perkin-Elmer, Eden Prairie, MN, 1992.
35. Wilson, G. R., and Hall, W. K., *J. Catal.* **17**, 190 (1970).
36. Bartholomew, C. H., and Farrauto, R. J., *J. Catal.* **45**, 41 (1976).
37. Kasztelan, S., Grimblot, J., Bonnelle, J. P., Payen, E., Toulhoat, H., and Jacquin, Y., *Appl. Catal.* **7**, 91 (1983).
38. Wu, M., and Hercules, D. M., *J. Phys. Chem.* **83**, 2003 (1979).
39. Coenen, J. W. E., *Appl. Catal.* **75**, 193 (1991).
40. Daza, L., Pawelec, B., Anderson, J. A., and Fierro, J. L. G., *Appl. Catal. A* **109**, 167 (1992).
41. Scheffer, B., Molhock, P., and Moulijn, J. A., *Appl. Catal.* **46**, 11 (1989).
42. Rynkowski, J. M., Paryjczal, T., and Lenik, M., *Appl. Catal.* **106**, 73 (1993).
43. Arnoldy, P., de Jongue, J. C. M., and Moulijn, J. A., *J. Phys. Chem.* **89**, 4517 (1985).
44. Gil, A., Díaz, L. M., Gandía, L. M., and Montes, M., *Appl. Catal. A* **109**, 167 (1994).
45. Narayanan, S., and Uma, K., *J. Chem. Soc., Faraday Trans. 1* **84**, 521 (1988).
46. Narayanan, S., and Sreekanth, G., *J. Chem. Soc., Faraday Trans. 1* **85**, 3785 (1989).
47. Anderson, J. A., Daza, L., Fierro, J. L. G., and Rodrigo, T., *J. Chem. Soc., Faraday Trans. 1* **89**, 3651 (1993).
48. Stanislaus, A., and Cooper, B. H., *Catal. Rev. Sci. Eng.* **36**, 75 (1994).
49. Girgis, M. J., and Gates, B. C., *Ind. Eng. Chem. Res.* **30**, 2021 (1991).
50. Li, D., Nishijima, A., and Morris, D. E., *J. Catal.* **182**, 339 (1999).
51. Li, D., Nishijima, A., Morris, D. E., and Guthrie, G. D., *J. Catal.* **188**, 111 (1999).

52. Lin, S. D., and Vannice, M. A., *J. Catal.* **143**, 539 (1993).
53. Lin, S. D., and Vannice, M. A., *J. Catal.* **143**, 554 (1993).
54. Teixeira da Silva, V. L. S., Frety, R., and Schmal, M., *Ind. Eng. Chem. Res.* **33**, 1692 (1994).
55. Sepúlveda, J., and Fígoli, N. S., *React. Kinet. Catal. Lett.* **55**, 383 (1995).
56. Duprez, D., and Mendez, M., *Stud. Surf. Sci. Catal.* **34**, 523 (1987).
57. Kokayeff, P., "Catalyst Hydroprocessing of Petroleum Distillates," p. 315. Decker, New York, 1994.
58. Huang, T. C., and Kung, B. C., *Ind. Eng. Chem. Res.* **34**, 1140 (1995).
59. Ozkan, U. S., Zhang, L., Ni, S., and Moctezuma, E., *J. Catal.* **148**, 181 (1994)
60. Kabe, T., Qian, W., and Ishihara, A., *J. Catal.* **149**, 171 (1994).
61. Louwers, S. P. A., and Prins, R., *J. Catal.* **133**, 94 (1992).